Tandem Cylinder Aerodynamic Sound Control Using Porous Coating

Hanru Liu[a], **Mahdi Azarpeyvand**[b], **Jinjia Wei** [a]

[a] *State Key Laboratory of Multiphase Flow in Power Engineering, Xi'an Jiaotong University, Xi'an, PR China*

[b] *Department of Engineering, University of Cambridge, Cambridge, CB2 1PZ, United Kingdom*

ABSTRACT

This paper is concerned with the application of porous coatings as a passive flow control method for reducing the aerodynamic sound from tandem cylinders. The aim here is to perform a parametric proof-of-concept study to investigate the effectiveness of porous treatment on bare tandem cylinders to control and regularize the vortex shedding and flow within the gap region between the two bluff bodies, and thereby control the aerodynamic sound generation mechanism. The aerodynamic simulations are performed using 2D transient RANS approach with $k-\omega$ transitional turbulence model and the acoustic computations are carried out using the standard Ffowcs Williams-Hawkings (FW-H) acoustic analogy. Numerical flow and acoustic results are presented for bare tandem cylinders and porous-covered cylinders, with different porosities and thicknesses. Experimental flow and acoustic data are also provided for comparison. Results show that the proper use of porous coatings can lead to robust control of the flow within the gap region, the turbulence level and interaction with the downstream body, and therefore the generation of tonal and broadband noise. It has also been observed that the magnitude and the frequency of the primary tone reduce significantly as a result of the flow regularization. The proposed passive flow-induced noise and vibration control method can potentially be used for other problems involving flow interaction with bluff bodies.

Keywords: Tandem cylinders, porous material, vortex-shedding, acoustic resonance.

1. Introduction

The interaction of a uniform flow with two closely placed bodies produces strong unsteady aerodynamic forces which can then cause severe nonlinear vibration and excessive noise. The flow interaction with tandem structures is encountered in many applications, such as heat exchangers, twin cables in cable-stayed bridges, parallel bridges and landing gear system. Therefore, the aerodynamics, aero-acoustics and aero-elasticity of tandem structures have received considerable research attention over the past four decades [1-10]. In this paper, we shall focus on the aerodynamics and aero-acoustics of tandem cylinders and will examine a passive control method for regularization of the vortex shedding, reducing the unsteady loading and finally controlling the noise generation mechanism.

The flow around two cylinders in tandem represents an important and remarkably complex flow pattern and has been the subject of many experimental and numerical investigations [1, 2]. For flow interaction with tandem bodies (particularly cylinders), the separation distance plays a very important role and has profound effects on flow characteristics, within the gap and further downstream [3]. Concerning the unsteady aerodynamic forces, the problem of flow interaction with twin cylinders can be categorized as (1) wake-induced flutter: for cylinders located so far apart that there is essentially no interference and coupling between the two structures ($L/D > 10$), (2) wake-galloping: for cylinders with gap distance of $L/D < 5$, where there is strong interference between the structures [4]. In the latter case, studies have shown that unsteady effects of the flow within the gap region play an important role on the generation mechanism of the wake-galloping, unsteady loadings [5, 6] and thus the noise generation mechanism. In a

detailed experimental study, Zdravkovich investigated the dependence of vortex shedding on the arrangement of two cylinders through wind-tunnel experiments [7]. It was found that for a pair of cylinders with a small gap distance (below a critical value), the shear layer originating from the upstream cylinder reattaches on the downstream cylinder directly and therefore no vortex shedding occurs within the gap region. Also, Lin *et al.* [8] observed using PIV measurements at $Re = 1 \times 10^4$ the presence of Kelvin-Helmholtz instabilities from the separated shear layer of the upstream cylinder, which, in turn, influences the flow separation on the downstream cylinder. An extensive review on flow interaction with tandem cylinders can be found in Zdravkovich [3, 9] and Sumner [10]. Although these studies revealed some interesting properties of the flow and vortex shedding, the issue of noise generation mechanism, which is directly related to the unsteady characteristics of the flow, did not received much attention.

One important experimental research on tandem cylinder flow and noise has recently been carried out by NASA Langley Research Centre at the Basic Aerodynamic Research Tunnel (BART) and Quiet Flow Facility (QFF) [11-13]. It has been observed for tandem cylinders with the separation distance of $3.7D$ that both cylinders exhibit shedding, resulting in a strong interaction within the gap region and it was concluded that this relatively simple geometry involves complex noise generation physics [14]. Based on the experiment carried out at NASA [11-13], Khorrami *et al*. [15] initially performed two-dimensional, fully turbulent simulations using unsteady Reynolds Averaged Navier-Stokes (URANS) method to study the flow behavior around the tandem cylinders and the mechanism of noise generation. Time-averaged and unsteady flow characteristics were investigated and an overall reasonable agreement with

measurement was achieved, although failed to accurately predict some details, such as the gap velocity and pressure fluctuations on the downstream cylinder. Later, Lockard *et al.* [16] and Khorrami *et al*. [17] further extended the simulations to three dimensions, with limited spanwise length, and obtained improved flow features with some small-scale information. The far-field acoustic results have also been obtained using the Ffowcs-Williams and Hawkings (FW-H) method, which have shown good agreement with the measured data [13]. In a later study, Uzun and Hussaini [18] performed Delayed Detached Eddy Simulation (DDES) of flow past tandem cylinders with $L/D = 3.7$ separation distance. The mesh resolution used was in the order of 133 million grid points to produce fairly reliable results. However, they also pointed out that the limitation of affordable grid resolution, finite spanwise length, turbulence modeling errors and uncertainties in the measurement are likely causes for comparison discrepancies. Furthermore, Brès *et al.* [19] made use of the Lattice Boltzmann Method (LBM) and the standard FW-H acoustic analogy to predict the flow and noise of tandem cylinders, originally reported in Refs. [11-13]. A comprehensive review on computational efforts for modeling of the flow around tandem cylinders and noise radiation is provided by Lockard [14].

For many flow-induced noise problems of industrial importance, controlling the flow is regarded as the most effective way of suppressing the aerodynamic noise [20-22]. The classical categorization of bluff-body flow control method falls into passive and active methods [20-22]. The active control method requires auxiliary energy input and monitoring sensors. In contrast, the passive control is an easy and cheap method to implement with high robustness. However, passive methods normally require a parametric study which can be tedious, but necessary for an effective and robust performance. Some common passive methods for controlling the flow

around cylinders are: splitter plate behind the cylinder, vortex generator and longitudinal groove [22]. Using porous material treatments, *e.g.* open-cell metal foams, is another approach to manipulate and stabilize the flow. Revell *et al*. [23], Khorrami and Choudhari [24] have studied the application of porous treatments to reduce noise from flaps and slat trailing edges, respectively, and the results indicate that the aerodynamic noise can be reduced significantly by effective manipulation of the flow using porous treatments. Bruneau and Mortazavi [25, 26] used Direct Numerical Simulation (DNS) to show the ability of porous medium to regularize the flow around bluff bodies and reduce drag forces. Angland and Zhang [27] have also performed wind-tunnel experiments to investigate the effects of porous-treated flap side-edges on vortex shedding and airframe noise. Moreover, Sueki *et al.* [28] has experimentally demonstrated significant noise reduction using open-cell metal foam wraps for stabilizing the vortices and shear layer of the wake flow of an isolated single circular cylinder. More recently, Liu [29] carried out some numerical parametric studies for the application of porous coatings for noise reduction from an isolated cylinder and provided encouraging comparisons with experimental observations [28]. It is worth mentioning here that the numerical studies of Naito and Fukagata for a single cylinder [30] have shown that porous treatments for flow control are more effective at high Reynolds numbers. As mentioned earlier, most of these researches have mainly been focused on the aerodynamics of isolated cylinders and there are few studies on the issue of flow control for tandem structures, not to mention aerodynamic noise control. The underlying physics of the noise generation and also noise control is also not yet properly understood and requires more numerical and experimental research.

The remainder of the paper is organized as follows: Section II presents the methodology used here for modeling the flow and calculating the noise. The geometry of the tandem cylinders considered in this paper and the mesh details are provided in Sec. II. The URANS CFD model, the FW-H method for calculating the noise and the experimental setup, used at NASA test facility, are also briefly explained. Sections III is devoted to the results and discussions. Acoustic results will be presented first and comparisons will be made against the NASA measured data. To better understand the noise generation mechanism, results will also be provided for the effects of porous coatings on vortex shedding, steady and unsteady flow quantities and pressure loading on cylinders.

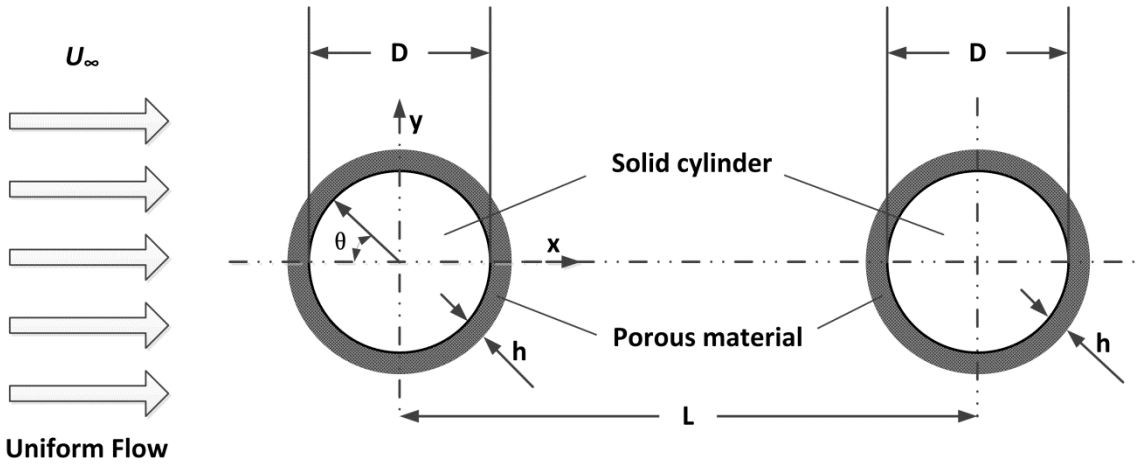

Figure 1. Schematic of the tandem cylinders structure with porous covers in a uniform flow.

2. Methodology

In the present work, the tandem cylinder arrangement and the flow condition are the same as those used in NASA flow and noise experiment [14]. The schematic of the tandem cylinder configuration with the porous coatings is shown in Fig. 1. The diameter of both rigid cylinders is $D = 0.05715\,m$ and the separation distance is $L = 3.7D$ [14]. The two cylinders are placed in a uniform flow, parallel to the center-to-center line, with a Mach number of 0.128. The corresponding Reynolds number, based on the inflow velocity U_∞ and solid cylinder diameter D is 1.66×10^5. Also, the non-dimensional thickness of the porous coating is defined as h/R, where h is the porous coating thickness and R is rigid core radius ($R = D/2$). Two-dimensional URANS approach, similar to the method used in [15], is utilized to simulate the flow around the tandem cylinders. The commercial FLUENT software [31] using finite volume method is employed to solve the incompressible unsteady Navier-Stokes and continuity equation. The two-equation shear stress transport (SST k–ω) model of Menter is used [32]. All current computations are performed using the second-order implicit time discretization and the

dual time-stepping method. The convective and diffusive terms were evaluated using the second-order upwind method and central difference with second-order accuracy, respectively. Although the flow in this problem is intrinsically three-dimensional, the two-dimensional approach can still capture some of the important flow characteristics (*e.g.* vortex shedding and wake) at a reduced computational cost [15] and is a more suitable method for a parametric study. The C-type computational domain, used for these simulations, contains in the order of 500,000 grid points, see Fig. 2. For bare (rigid) cylinders, no-slip boundary conditions are applied to the surfaces of the cylinders. The porous boundary condition will be explained later. The unsteady CFD simulations are performed with a non-dimensional time-step of $\Delta t U_\infty / D = 0.007$, such that the Courant-Friedrichs-Lewy (CFL) number is smaller than one almost over the entire computational domain. To calculate the unsteady flow quantities and sound pressure signals, a total number of 50,000 time steps of data are also collected, once the flow reaches the statistical steady-state.

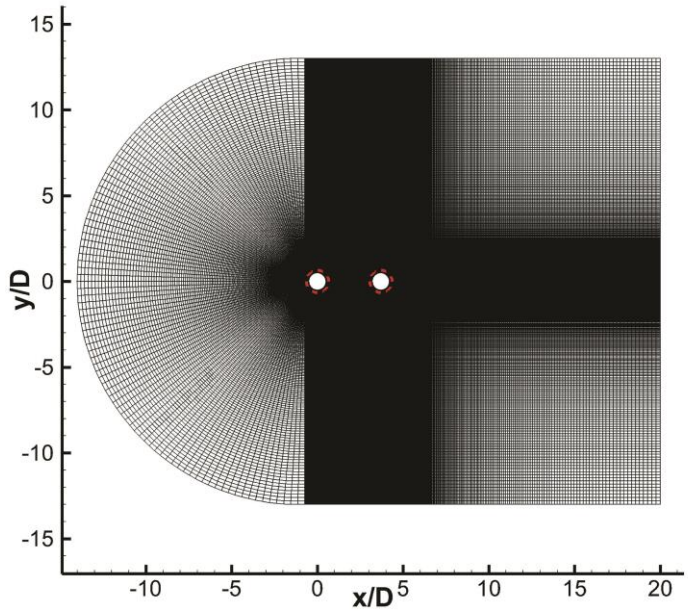

Figure 2. The C-type computational domain used for bare and porous-covered tandem cylinders.

Table. 1 Comparison of flow properties between simulations and experiment for NASA bare tandem cylinders

Case	Cells	$\bar{C}_{D,up}$	$\bar{C}_{D,down}$	$C'_{L,up}$	$C'_{L,down}$	Vortex shedding frequency (St)
2D simulation [15]	401,000	0.71	0.32	0.72	1.35	0.237
3D simulation [16]	60,000,000	0.43	0.52	0.049	0.421	0.219
Experiment [12]	-	0.59-0.63	0.24-0.35	-	-	0.231-0.234
Present URANS simulation	500,000	0.79	0.30	0.64	1.31	0.234

A comparison of the calculated mean and root-mean-square flow quantities for a pair of rigid cylinders with $L/D = 3.7$ against some of the earlier numerical and experimental studies is provided in Table 1. The comparison of the current URANS simulations with other 2D simulations [15] and experimental data shows that the employed in this paper can capture the vortex shedding frequency tone (primary tone) with very good accuracy. The drag coefficient on the downstream cylinder ($\bar{C}_{D,down}$) has also been found to be in good agreement with the experimental results, while that on the upper cylinder is slightly over-predicted, as previously shown and discussed in Ref. [15]. Also, the 2D URANS simulation over-predicts the root-mean-square of the unsteady lift coefficients ($C'_{L,up}$), compared to 3D numerical study [16]. This is mainly due to the inaccurate evaluation of the flow separation position and the inherent weaknesses of two-dimensional approaches.

In these simulations, the porous material is assumed to be homogeneous and the flow outside the porous medium is simulated by solving the normal continuity and Navier-Stokes equations. The Brinkman-Forchheimer extended Darcy model is used to describe the mass and

momentum conservation in the porous medium, similar to Vafai [33] and Hsu and Cheng [34], as follows:

$$\nabla \cdot \mathbf{u}_D = 0\,, \tag{1}$$

$$\rho\left[\frac{\partial \mathbf{u}_D}{\partial t} + \nabla \cdot \left(\frac{\mathbf{u}_D \mathbf{u}_D}{\phi}\right)\right] = -\nabla P + \mu \nabla^2 \mathbf{u}_{\mathrm{D}} - \left[\frac{\mu \phi \mathbf{u}_D}{K} + \frac{C_F \rho \phi \mathbf{u}_D |\mathbf{u}_D|}{\sqrt{K}}\right], \tag{2}$$

where, $\mathbf{u}_D = \phi\langle \mathbf{u} \rangle^{\mathrm{i}}$ is the Darcy velocity, $\langle \mathbf{u} \rangle^{\mathrm{i}}$ is the intrinsic (liquid) average of local velocity vector and ϕ is the porosity (above 0.80 in this paper), ρ and μ are, respectively, the density and the dynamic viscosity of the fluid. Also, $P = \phi\langle \mathrm{p} \rangle^{\mathrm{i}}$, where $\langle \mathrm{p} \rangle^{\mathrm{i}}$ is the intrinsic average pressure of the fluid. The turbulence quantities within the porous material are treated in the same way as in the standard conservation equations outside the porous medium, which is a reasonable approximation for highly porous media. Also, the permeability K and inertia coefficient C_F (or Forchheimer coefficient) of the porous medium are expressed as [33, 35],

$$K = \frac{d_p^2 \phi^3}{150(1-\phi)^2}, \tag{3}$$

$$C_F = \frac{1.75}{\sqrt{150}\phi^{3/2}}, \tag{4}$$

where d_p is the particle diameter, as defined by Ergun [36] and the Darcy number can also be defined as $\mathrm{Da} = K/D^2$. The method used to model the flow transport within the porous material in this paper is similar to that of Bhattacharyya and Singh [37], Bae and Moon [38] and Bae *et al.* [39].

For computing the radiated aerodynamic noise, the computational fluid dynamic (CFD) results are used as input to the Ffowcs Williams–Hawkings (FW–H) solver [40]. In order to use the two-dimensional near-field flow data, a "correlation length'' method is adopted, as per Refs. [31, 41]. This method assumes that the vortex shedding is perfectly correlated over a certain

length of the cylinder in the spanwise direction. The FW–H integrals will then be evaluated over this length using the identical source data acquired from the CFD calculation, which means the source volume is built with the specified span-length and the sources outside this region are neglected. In this paper, the correlation length of five times the cylinder diameter is chosen, following Refs. [41, 42]. The FW-H integral surface is defined on the surface of the cylinders. Since the flow Mach number is very low, ignoring the quadrupole sources in the surrounding turbulent flow will not have a significant effect, as discussed by Lockard *et al.* [16].

3. Results and Discussions

In this section we shall provide flow (steady and unsteady) and acoustic results for bare (untreated) and porous-covered (treated) tandem cylinders. As mentioned earlier, the flow results have been calculated using an URANS solver and the acoustic data are obtained using the FW-H method. The main objectives of the following sections are to firstly provide a proof-of-concept study for the application of porous treatments for vortex-shedding control and suppression of vortex-shedding associated sound, in particular for tandem cylinder configuration, and secondly, to better understand the underlying physics of such passive flow/noise control methods by studying various steady and unsteady flow characteristics. In the following subsection, we shall provide results for (1) acoustic, (2) steady and unsteady aerodynamic forces, and (3) flow characteristics for tandem cylinder configuration.

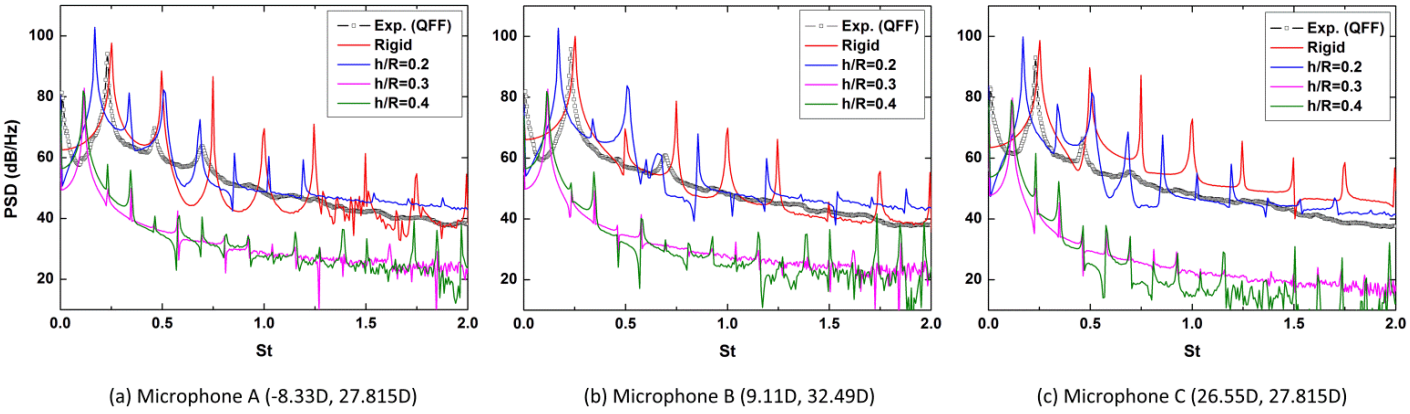

Figure 3. The effect of thickness of the porous coating on the noise from tandem cylinders.

3.1. Acoustic results

In order to illustrate the effectiveness of porous coatings for reducing aerodynamic noise, the radiated noise has been calculated using the URANS/FW-H method. Figure 3 presents the noise results for bare and porous-covered tandem cylinders with porosity of $\phi = 0.95$, Darcy number of $\mathrm{Da} = 7.86 \times 10^{-3}$ and thickness of $h/R = 0.2$, 0.3 and 0.4 at three microphone locations. Microphone A is positioned at (-8.33*D*, 27.815*D*), microphone B at (9.11*D*, 32.49*D*) and microphone C at (26.55*D*, 27.815*D*) relative to the centre of the upstream cylinder. The QFF [13] measured power spectrum density (PSD) results for bare twin cylinders are also provided for comparison. An inspection of the results in Fig. 3 shows that the results obtained using the URANS/FW-H method are in good agreement with the measured data, particularly for capturing the primary tonal frequency, the correct amplitude of the primary tone and the overall broadband PSD pattern. This implies that the URANS/FW-H method utilized is able to capture the most important sound generation mechanisms, *i.e.* vortex shedding and interaction, and also has the potential to offer added insight through a parametric study. A comparison of the present URANS/FW-H simulated results with various other 2D and 3D numerical simulations [14] and

measured data [13] is provided in Fig. 4. The obvious discrepancy between different simulations shows that the accurate prediction of the radiated noise from tandem cylinders using a CFD-based method is a challenging problem, as discussed by Lockard [14]. Returning to Fig. 3, the use of a thin porous treatments ($h/R < 0.2$) does not lead to a significant noise reduction. However, the use of a thicker porous coating ($h/R \geq 0.3$) results in a noticeable reduction in the frequency of the primary tonal noise from $St = 0.24$ (rigid) to $St = 0.12$ (porous) and the broadband noise level reduction of up to 15 dB. The significant changes to the tonal and broadband noise indicate that important changes have occurred in the flow pattern, vortex shedding and the vortex impingement on the secondary cylinder. This will be further discussed in the following two subsections.

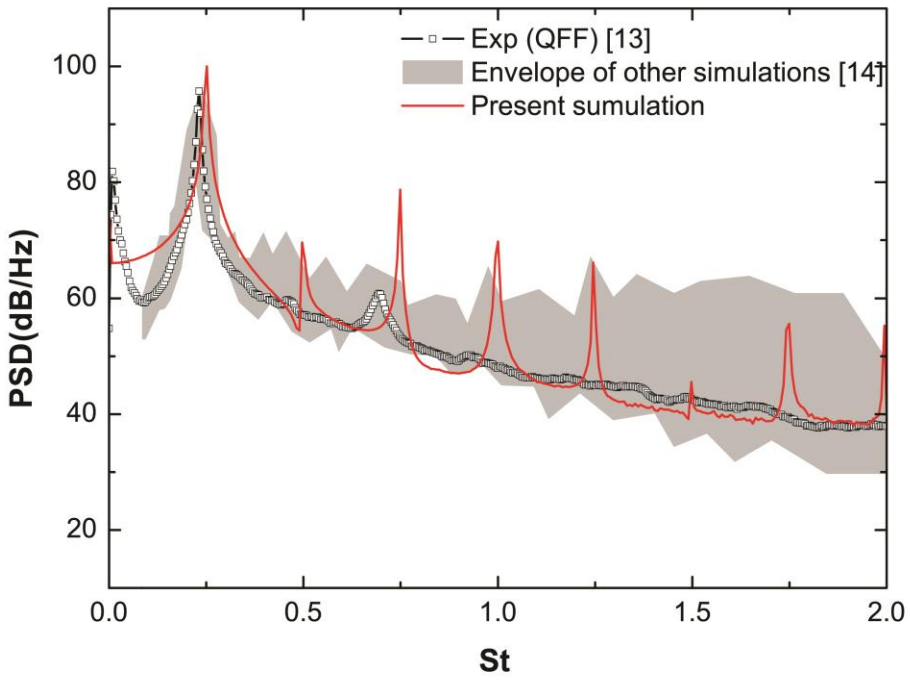

Figure 4. Comparison of noise spectra at Microphone B (9.11*D*, 32.49*D*) collected from various experimental and numerical investigations.

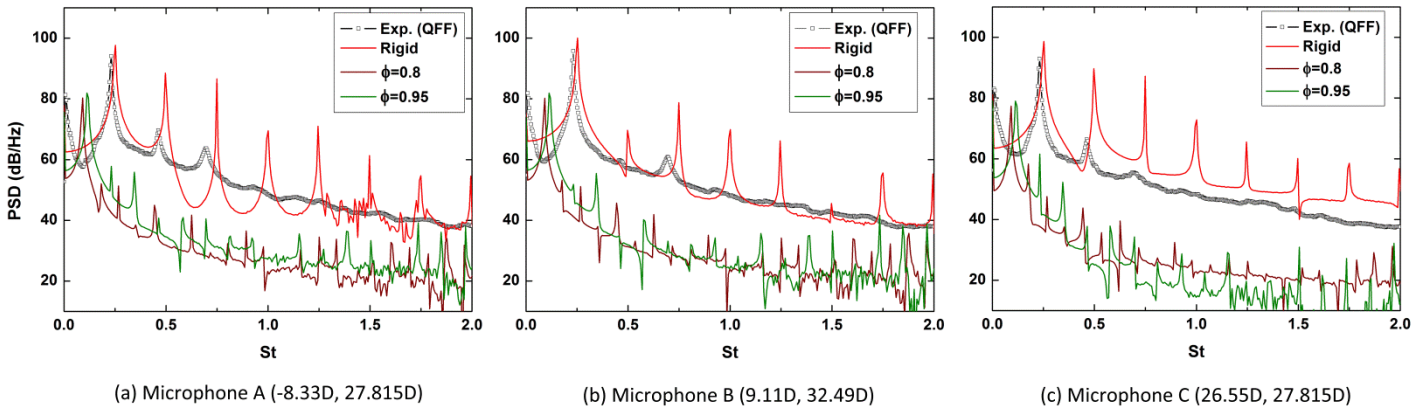

Figure 5. The effect of porosity of the coating on the noise from tandem cylinders.

Earlier studies have shown that the effectiveness of flow control using porous materials is strongly dependent upon the porosity of the treatment. Prior numerical and experimental studies on the application of porous treatments for vortex shedding control from isolated cylinders have shown that effective flow regularization can be achieved using highly porous materials, *e.g.* Bruneau and Mortazavi [25, 26]: ϕ close to 1, Sueki *et al.* [28]: $\phi = 0.97$, Zhao and Cheng [43]: $\phi = 0.8$ and Naito and Fukagata [30]: $\phi = 0.95$. In order to study the effects of the porosity of the coatings, two different porosities, $\phi = 0.8$ and 0.95, are considered. Figure 5 shows that the PSD spectra for treated and untreated cylinders at three microphone locations. Results show that within this high porosity range ($\phi > 0.8$), the noise amplitude is reduced significantly both at the first dominant tonal frequency and the overall broad frequency range. Finally, to better demonstrate the noise reduction levels at each microphone location, the overall sound pressure level (OASPL) results are also provided for the bare and porous-covered cylinders, see Fig. 6. The calculated OASPL results for the rigid case are over-predicted by 2 dB compared to the QFF measured data. The radiated noise from tandem cylinders with a thin porous coating ($h/R = 0.2$) is quite similar to that of the rigid cylinders. The thicker porous coatings, on the

other hand, can reduce the radiated noise by up to 15 dB. Results have also shown that the change of porosity (in the high porosity range) for thick coatings ($h/R = 0.4$), does not significantly improve the noise reduction.

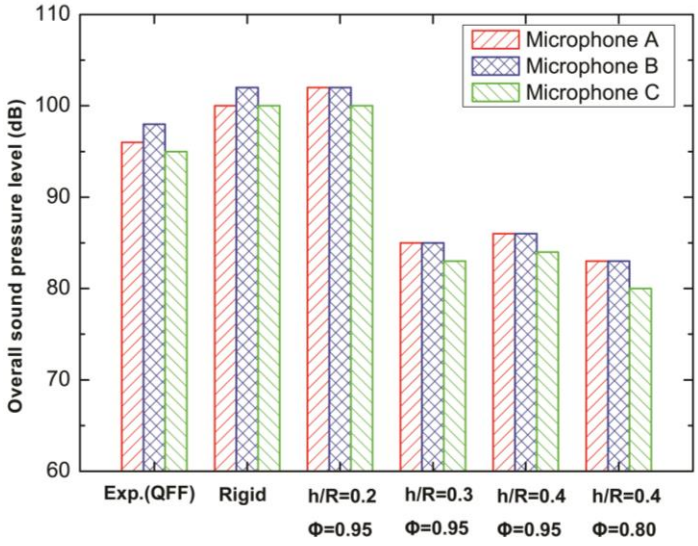

Figure 6. Overall sound pressure level for tandem cylinder configuration with and without porous coating at three microphone positions: Microphone A at (-8.33D, 27815D), Microphone B at (9.11D, 32,49D) and Microphone C at (26.55D, 27.815D).

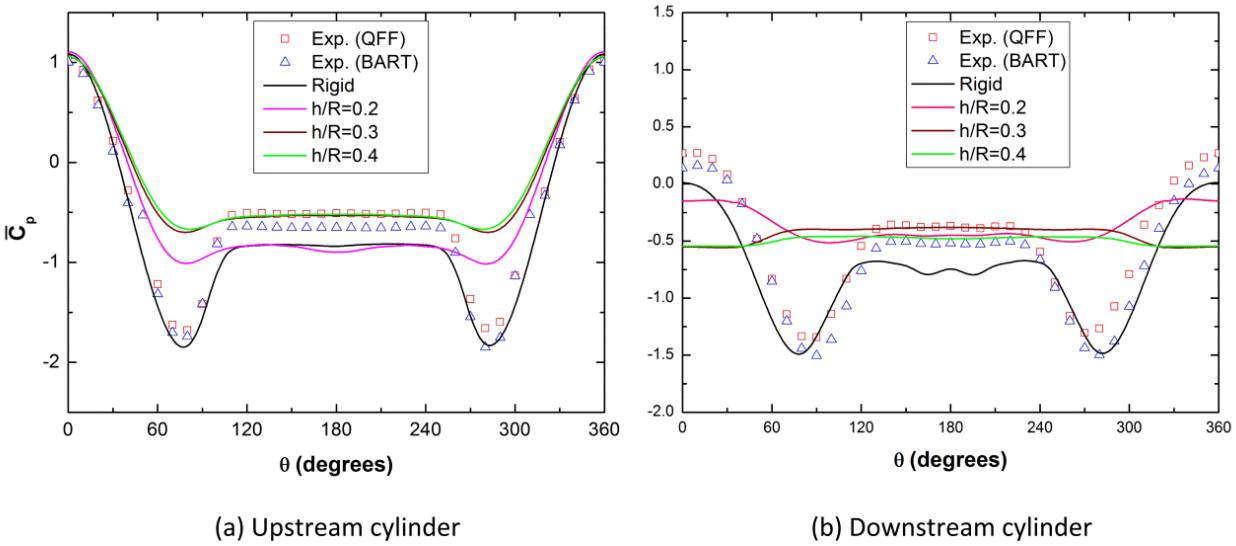

Figure 7. Time-averaged surface pressure coefficients on (a) upstream cylinder and (b) downstream cylinder.

3.2. Steady and unsteady aerodynamic forces

As shown in the previous section, using porous coating can significantly reduce the noise radiation, which is believed to be due to the changes to the structure of the flow between the cylinders and flow interaction with the downstream cylinder. To better understand the underlying physical mechanisms, we need to analysis the steady and unsteady aerodynamic forces and flow features around the cylinders, with and without the porous treatment. Since the noise reduction is not a strong function of the porosity at high porosity range, as seen in Figs. 5 and 6, we shall only use $\phi = 0.95$ for our analysis here.

Figure 7 displays the time-averaged pressure coefficient distribution ($\bar{C}_p$) on the upstream and downstream cylinders, over $0^\circ < \theta < 360^\circ$ (as defined in Fig. 1). Two sets of experimental data [11-13] are also provided for comparison. The pressure coefficient distributions on rigid cylinders show good overall agreement with experimental data [11-13]. The base-pressure, C_{pb}, (*i.e.* pressure around 180º from the stagnation point) and the location of the suction peak and stagnation pressure of the downstream cylinder are slightly under-predicted. The discrepancies are attributed to the lack of three-dimensional effects in these simulations and a slight flow angularity in the experiment [15, 44]. The two symmetric suction areas appearing in the case of rigid cylinders, for both cylinders, disappear gradually with increasing the thickness of the porous coating layer. In Fig. 7-a, for the upstream cylinder, the base-pressure (C_{pb}) increases by adding the porous coating and becomes more evident for thicker coatings ($h/R > 0.2$). For the porous-covered cylinders, the higher front-side pressure of the upstream cylinder ($40^\circ \leq \theta \leq 80^\circ$) results in an increase of the drag coefficient, $\bar{C}_{D,up}$, compared to the rigid case. Results in Fig. 7-b, for the downstream cylinder, show that the pressure distribution on porous-covered cylinders,

particularly $h/R = 0.3$ and 0.4, becomes nearly flat and the pressure on the rear-side is higher than that on the front-side. This results in a net axial force in the opposite direction of the flow, *i.e.* an axial pulling force. These will be further discussed in Fig. 8 and Table 2.

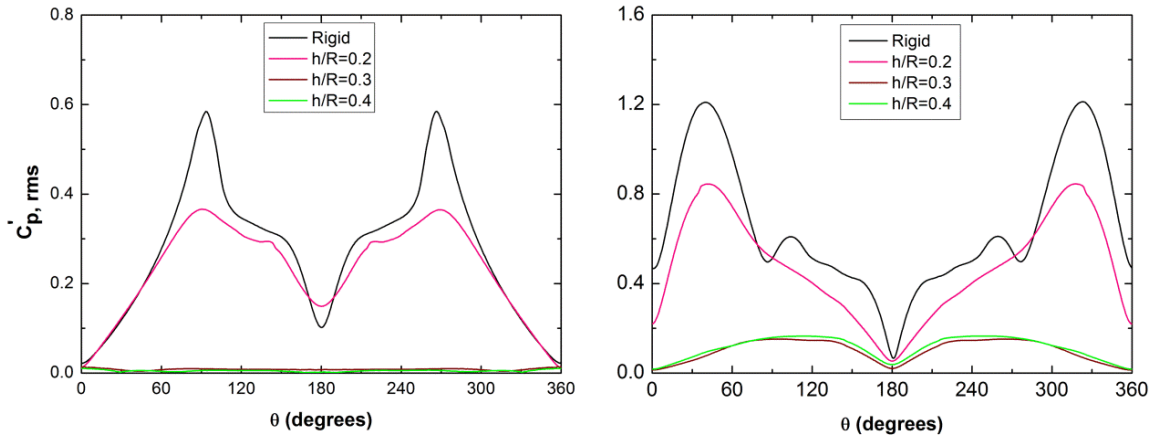

Figure 8. RMS of surface pressure coefficients on (a) upstream cylinder and (b) downstream cylinder.

Figures 8-a and 8-b present the root-mean-square (RMS) of the unsteady surface pressure coefficients,C_p', for the upstream and downstream cylinders, respectively. The results of the upstream cylinder, Fig. 8-a, show that for the rigid and thin porous coating ($h/R = 0.2$) cases, a distinct single peak arises at around 90º (and 270º), which is associated with flow separation in this region. Results have shown that the use of the thicker porous coatings ($h/R > 0.2$) causes a strong reduction in the RMS magnitude of the unsteady pressure fluctuations over the entire surface of the upstream cylinder. Figure 7-b presents the RMS surface pressure coefficient results on the downstream cylinder, with and without porous treatment. The C_p' profile on the downstream cylinder shows a dual peak behaviour for the rigid case. As explained in Ref. [16], the first prominent peak occurring at around 40º (and 320º) is the result of the upstream wake impingement on the front-side of the downstream cylinder, while the second less peak at around

100º (and 260º) is due to the boundary layer separation. In the case of cylinders covered with $h/R = 0.2$ porous cover the only peak is due to the flow impingement and the boundary layer separation point vanishes due to the boundary conditions and flow injection into the surrounding medium through the porous surface (this can be better seen in Figs. 10 through 12). For cylinders covered by a thick porous coating ($h/R > 0.2$), the RMS surface pressure coefficient is much smaller than that of the bare cylinders. The RMS surface pressure on the downstream cylinder peaks over a large area ($70^\circ \leq \theta \leq 140^\circ$ and $220^\circ \leq \theta \leq 290^\circ$). It will be explained later (Fig. 10) that this flat peak area is, in fact, due to the emergence of two strong wake regions at the front- and rear-sides of the downstream cylinder and not the flow impingement, nor the boundary layer separation.

The comparison of the results in Figs. 8-a and 8-b also show that the downstream cylinder exhibits higher fluctuation levels than the upstream cylinder, due to the interaction with the wake of the upstream cylinder. One can, therefore, conclude that the level of fluctuations on the downstream cylinder is related to the turbulence level of the impinging flow and thus what occurs on the upstream cylinder. Higher levels of fluctuations on the upstream cylinder will bring about higher levels on fluctuations on the downstream cylinder. However, this process is quite nonlinear and there is no one-to-one correspondence between the fluctuation levels on the upstream and downstream bodies, as previously mentioned in Ref. [16]. The significant attenuation of the surface pressure fluctuations on both cylinders when using porous coating with sufficient thickness leads to the suppression of the lift fluctuations, directly related to the dipole radiated noise [45]. Therefore, careful control of the vortex shedding within the gap region could prevent, or at least improve the noise radiation by reducing the vortex impingement

on the front-side of the downstream cylinder. From the acoustic results in Figs. 3 through 5, we have known that thick porous coatings ($h/R > 0.2$) with high porosity ($\phi > 0.8$) should achieve this aim.

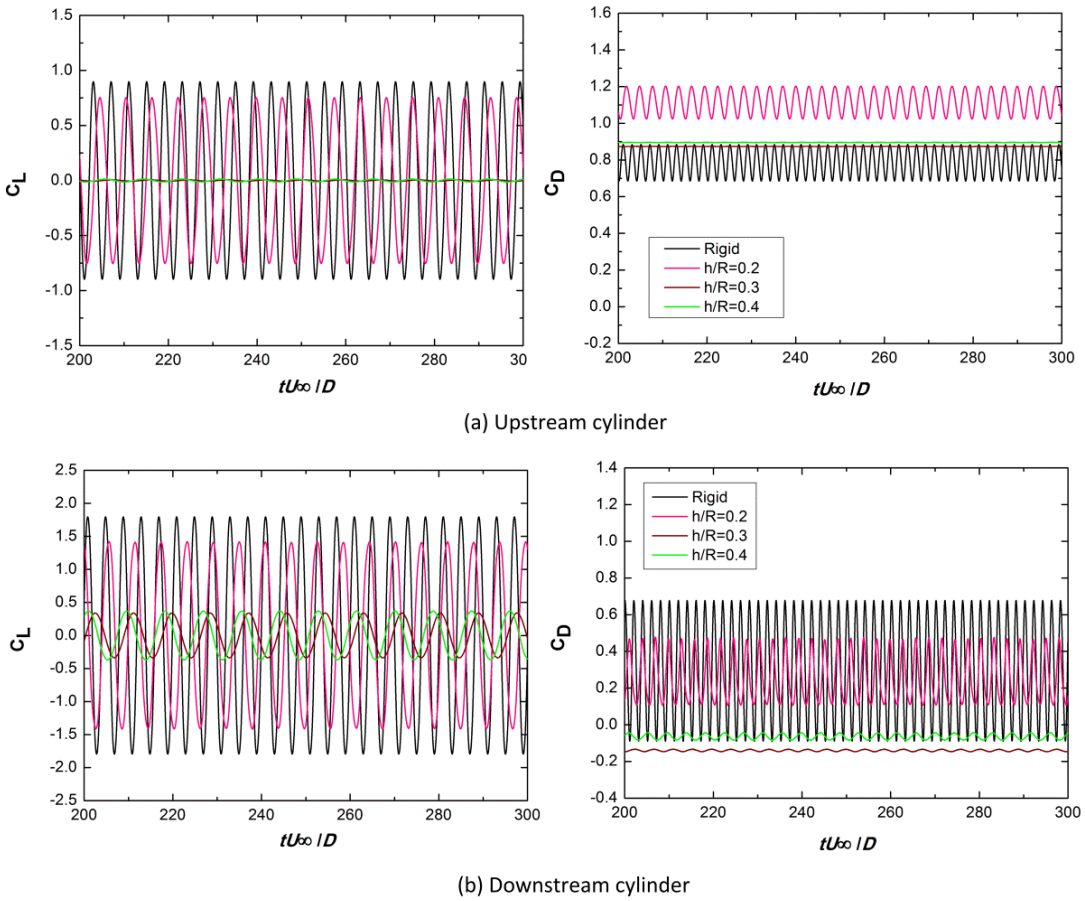

Figure 9. Time history of lift and drag coefficients on (a) upstream cylinder and (b) downstream cylinder.

The time-history of the lift and drag coefficients (C_L and C_D) on both cylinders obtained from the present 2D URANS simulations are presented in Fig. 9 as a function of non-dimensional time, tU_∞/D. In this paper, only the drag due to the pressure difference (vortex-drag) is considered. Due to the high Reynolds number involved, the viscous-drag component can be ignored. As seen in Fig. 9, the force signals are periodic and statistically stationary. For the upstream cylinder, the fluctuations of the lift coefficient seem to decrease

significantly by adding the porous coating of thickness $h/R = 0.3$ and 0.4 and the curves are nearly flat compared to the untreated bare rigid case. The use of a thin coating ($h/R = 0.2$), on the other hand, leads to a very little reduction of the lift fluctuations. The drag coefficient fluctuations of the upstream cylinder also decrease by the porous coating, although the mean drag coefficient, $\bar{C}_{D,up}$, shows a slight increase. In the case of thin porous covers ($h/R = 0.2$), however, the drag on the upstream cylinder increases compared to bare cylinders, which is due to surface pressure distribution, as discussed for Fig. 7. The mean and fluctuation values of the aerodynamic forces and the normalized primary tonal frequency Strouhal number ($St = fD/U_\infty$) are summarized in Table 2. The time-history of the lift coefficient for the downstream cylinder also shows similar trends. The only difference is that the fluctuation magnitude is larger than that for the upstream cylinder. This was also reflected in our RMS surface pressure distribution results in Fig 8. Furthermore, it is noticed that the drag coefficient and fluctuations of the downstream cylinder are considerably reduced when the porous treatment is applied with sufficient thickness ($h/R > 0.2$). As observed in Table 2, the mean drag coefficient on the downstream cylinder, $\bar{C}_{D,down}$, decreases even to negative values for porous-covered cases with $h/R \geq 0.3$. This means that the net horizontal force acting on the cylinder pulls the object upstream (in the opposite direction of the flow), as per the discussion for Fig. 7-b. The drag reduction is due to the significant changes to the pressure distribution over the downstream cylinder, which itself stems from the changes to the shape and location of the upstream wake, as well as the wake behind the downstream cylinder.

As mentioned earlier for Figs. 3-5, the frequency of the primary tone decreases with the porous treatment thickness, thanks to the effective regularization of the vortex shedding from the

upstream cylinder. This will be better illustrated later in our contour plots of the mean and unsteady quantities, see Figs. 10-13. Based on the results in Figs. 8 and 9 and using Curle's theory of aerodynamic-noise [45], one can conclude that controlling of the vortex-impingement on the downstream cylinder reduces the unsteady pressure and lift fluctuations, which, in turn, will reduce the noise radiation from the system, as per the acoustic results in Figs. 3 through 5.

Table. 2 Comparison of flow properties between rigid case and porous coating cases with various porous thicknesses.

Case	$\bar{C}_{D,up}$	$\bar{C}_{D,down}$	$C'_{L,up}$	$C'_{L,down}$	St
Rigid (baseline)	0.79	0.30	0.64	1.31	0.234
Porous (ϕ=0.95, h/R=0.2)	1.116	0.259	0.538	1.049	0.169
Porous (ϕ=0.95, h/R=0.3)	0.87	-0.14	0.004	0.24	0.117
Porous (ϕ=0.95, h/R=0.4)	0.90	-0.064	0.009	0.263	0.117

3.3. Flow characteristics

The mean flow streamlines superimposed on the time-averaged total velocity magnitude, normalized by U_∞, are presented in Fig. 10, where the solid lines represent the solid surface of the bare cylinders and the white dashed-lines represent the porous covers. Figure 10-a shows the results for the untreated rigid cylinders and Figs. 10-b through 10-d show the results for tandem cylinders with porous coating with thickness of $h/R = 0.2,\ 0.3$ and 0.4, respectively. In the case of bare rigid cylinders, Fig. 10-a, two short recirculation regions (vortex pairs) appear behind the upstream and downstream cylinders. The wake from the upstream cylinder closes in the gap region and two cylinders shed almost independently. The overall flow features of the rigid

cylinders observed in Fig. 10-a are in very good agreement with the PIV observations, see Figs. 8-a, and 13-c in Ref. [11], and other independent numerical investigations [15, 18]. In the case of a thin porous coating ($h/R = 0.2$), there is a similar recirculation region behind the upstream cylinder, closing within the gap region between the two cylinders, see Fig. 10-b. However, the vortex pair behind the downstream cylinder now occupies a larger lateral and longitudinal space, with the vortex centres located further downstream, relative to the rigid case.

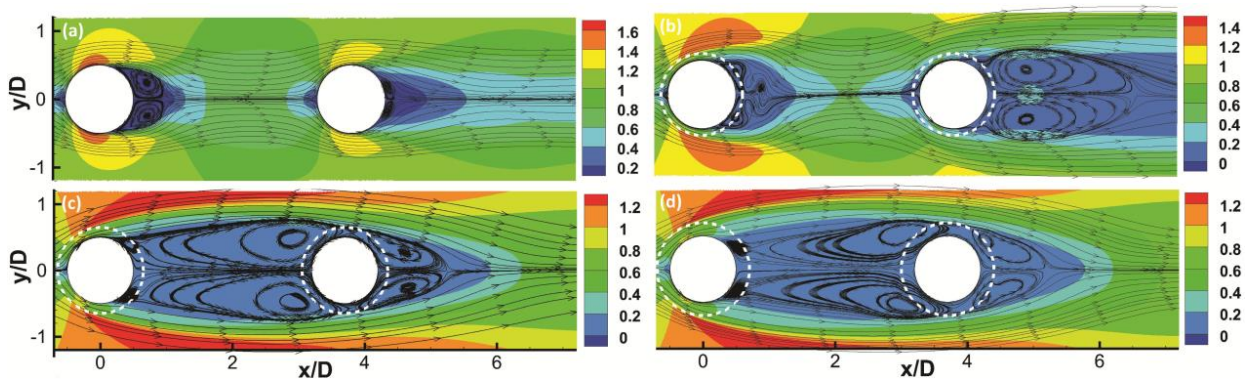

Figure 10. Mean flow streamlines superimposed on total velocity magnitude normalized by U_∞ for (a) rigid case, (b) $h/R = 0.2$, $\phi = 0.95$, (c) $h/R = 0.3$, $\phi = 0.95$, (d) $h/R = 0.4$, $\phi = 0.95$.

The flow velocity patterns around porous-covered tandem cylinders with thickness of $h/R = 0.3$ and $h/R = 0.4$, in Figs. 10-c and 10-d, show an overall similarity between the two cases. The most important effect of the porous treatment is the changes in the formation and the spatial-extent of the vortices from the upstream cylinder. Results show that the main vortex pair is now formed further downstream, occupying the whole gap region, with the vortex-centres very close to the front-side of the downstream cylinder. The magnitude of the flow velocity within the gap, however, is less than that of the bare tandem cylinders. Since vortex cores are associated with low-pressure regions, a lower pressure distribution on the front-surface of the downstream cylinder and higher pressure distribution on the rear-surface of the upstream

cylinder is expected. This is consistent with the results in Fig. 7 that using a thick porous coating will cause the base-pressure (C_{pb}) of the upstream cylinder to increase and the pressure on the front-side ($0° \leq \theta \leq 50°$ and $310° \leq \theta \leq 360°$) of the downstream cylinder to decrease. Moreover, the porous coating modifies the vortex pair behind the downstream cylinder, which causes the base pressure C_{pb} to increase on the downstream cylinder, as seen in Fig. 7. These two simultaneous actions produce a significant drag reduction on the downstream cylinder, as already observed in Fig. 9 and Table 2. Figure 10 also shows some interesting results regarding the injection of low velocity flow from the porous coating into the surrounding medium. The emergence of this low energy flow in the rear-side of the cylinder suppresses the formation of instabilities in the shear layers detaching from the upstream cylinder. Besides, the slip condition between the porous coating surface and the fluid is believed to weaken the flow shear and vortex shedding [25, 26, 30]. The results in Figs. 10-c and 10-d also show that the emergence of the flat peak RMS surface pressure region on the downstream cylinders, as seen in Figs. 8-c and 8-d, is primarily due to the appearance of two low pressure wake regions at the front- and rear-sides of the downstream cylinder. This is unlike the rigid tandem cylinder configuration, whose peaks have been attributed to the flow impingement and boundary layer separation [16]. The interaction between these two wake cores leads to the flat peak RMS surface pressure regions over $70^{\circ} \leq \theta \leq 140^{\circ}$ and $220^{\circ} \leq \theta \leq 290^{\circ}$ on the downstream cylinder, see Figs. 8-c and 8-d and Figs. 10-c and 10-d.

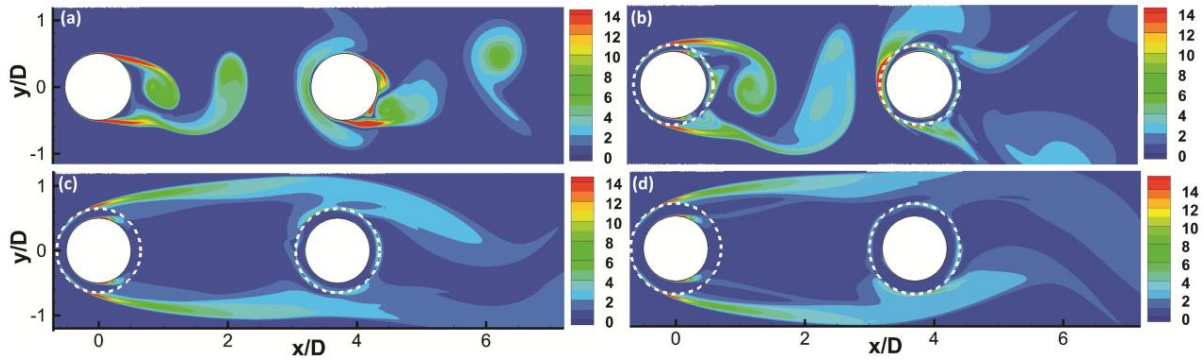

Figure 11. Instantaneous spanwise vorticity magnitude, $|\omega_z| D/U_\infty$ for (a) rigid case, (b) $h/R = 0.2$, $\phi = 0.95$, (c) $h/R = 0.3$, $\phi = 0.95$, (d) $h/R = 0.4$, $\phi = 0.95$.

Figures 11-a through 11-d show the normalized instantaneous spanwise vorticity field for rigid and porous-covered tandem cylinders over the magnitude range of $0 \leq |\omega_z| D/U_\infty \leq 15$. For the rigid case, Fig. 11-a, the intense large scale vortex shedding feature closely resembles the PIV measurements [11], but the small-scale scattered rolling-ups and vortices associated with the Kelvin-Helmhotz instability cannot, of course, be observed in these simulations, as previously discussed in Ref. [15]. For the rigid case and porous cover of $h/R = 0.2$, vortex shedding occurs on both the upstream and downstream cylinders. The vorticity fields in Figs. 11-a and 11-b clearly show the convection and impingement of the vortices with the downstream cylinder. For the porous cases with larger thickness ($h/R = 0.3$ and 0.4), as a consequence of the energy dissipation and low energy flow injection, the upstream vortex shedding is completely stabilized and no rolling-up occurs within the gap region. This phenomenon is similar to when the bodies are placed very close to one another (L/D is smaller than 2.5) [3, 7, 9, 10, 15]. The amplitude of the vorticity field also decreases significantly with h/R. This result is quite similar to the experimental observations of Sueki *et al* [28] at $Re = 4.7 \times 10^4$, numerical simulation of Liu [29] at $Re = 4.7 \times 10^4$, and Naito and Fukagata [30] at $Re = 5 \times 10^4$ for an isolated porous-covered circular cylinder. Results in Figs. 11-c and 11-d also shows that the shear layers

detaching from the upstream body pass over of the downstream cylinder surface (or weakly reattach to the downstream cylinder) behaving as an almost isolated cylinder vortex shedding with much lower shedding frequency, as seen in Table 2. Thus, it is possible to conclude that the strong interaction and coupling effects between the two cylinders are weakened significantly as a result of the passive flow control using the porous treatment.

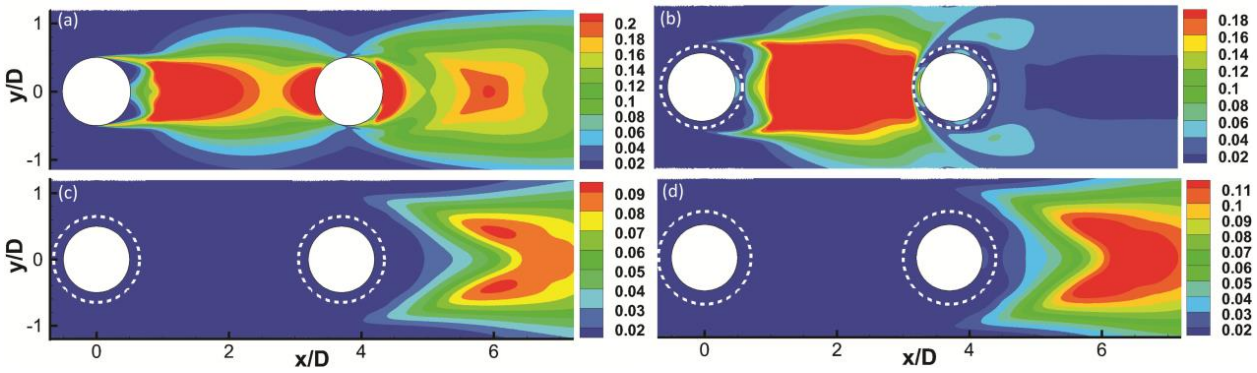

Figure 12. Mean turbulent kinetic energy normalized by U_∞^2 for (a) rigid case, (b) $h/R = 0.2,\ \phi = 0.95$, (c) $h/R = 0.3,\ \phi = 0.95$, (d) $h/R = 0.4,\ \phi = 0.95$.

Figure 12 shows the contours of the non-dimensional time-averaged turbulent kinetic energy (TKE) *i.e.* $1/2(\overline{u'u'} + \overline{v'v'})/U_\infty^2$ over $-1 < x/D < 7$ and $-1 < y/D < 1$. The comparison of the results in Fig. 12-a and the experimental observations [11] shows a very good agreement. Results in Fig. 12 have shown that the turbulence level within the gap region is highest for the bare rigid cylinders. The highest level of normalized TKE for bare cylinders and the $h/R = 0.2$ is in order of 0.2, which occurs within the gap region. The use of a thicker porous coating, however, significantly reduces the turbulence level within the gap region. The highest level of normalized TKE for the $h/R = 0.3$ and $h/R = 0.4$ cases are 0.09 and 0.11, respectively, which occur in the wake of the downstream cylinder. A comparison of the results in Figs. 10 through 12 suggests that the porous coating can significantly control the flow within the gap

region. It is well known that the coupling and interaction between the two cylinders, and therefore the noise radiation mechanism, depend strongly on the properties of the flow in the gap region. It is, therefore, possible to conclude that the effective control of the vortex shedding within the gap region using the porous coating can stabilize the flow, reduce the turbulence level in the gap region, reduce the unsteady lift fluctuations on the downstream cylinder, and finally significantly reduce the noise generation.

Finally, it is important to establish some conditions for the critical thickness of the porous coating (h/R), above which effective flow control (*i.e.* vortex shedding control) and significant noise reduction can be achieved. For isolated cylinders, Bruneau and Mortazavi [25, 26] suggested that for very thin ($h/R < 0.1$) the Darcy flow cannot be established inside the porous layer and the control is thus inefficient. Sueki *et al.* [28] and Naito and Fukagata [30] used very thick porous layers of $h/R = 0.8$ and $h/R = 1$ to obtain a clear flow control and noise reduction. Zhao and Cheng [43] and Liu *et al*. [29] indicated that the thicker the porous coating, the more efficient flow control becomes for isolated circular cylinders. Regarding tandem cylinders covered with porous layers of high porosity, our numerical investigations have shown that the critical porous layer thickness should be within the range of $0.2 < h/R < 0.3$. This can also be clearly seen in Figs. 10-12 for flow control and Figs. 3, 5, 6 for noise control.

4. Conclusions

The application of porous coating as a mean to control vortex shedding from tandem cylinders and hence the noise generation and radiation mechanism has been studied numerically. The flow characteristics around the bluff bodies have been studied using 2D URANS approach with k–ω SST transitional turbulence model, and the acoustic results have been obtained using the standard Ffowcs Williams-Hawkings acoustic analogy. The flow and acoustic results have also been compared with experimental data available in the literature. Numerical results for bare tandem cylinders have shown good agreement with measured flow and acoustic data. Regarding the application of porous coatings, results have shown that the vortex shedding from the upstream cylinder, and therefore the flow within the gap region, can be effectively controlled and stabilized using coatings with high porosity and relative thickness of $h/R > 0.2$. More importantly, the use of porous layer dampens the dominant tone and shifts it to lower frequency ranges. The overall broadband noise also decreased, up to 15 dB, as a result of stabilizing the vortex shedding and the turbulence within the gap region. The effects of the porous treatment on steady and unsteady aerodynamic forces, wakes and flow turbulence have also been investigated. The primary objective of this study was to provide a parametric proof-of-concept study for the application of porous treatments for flow-induced noise and vibration application. The detailed understanding of the flow characteristics and noise generation (and control) mechanisms require more in-depth CFD and experimental investigations.

Acknowledgements

The first author would like to acknowledge the financial support for his research at the University of Cambridge through the China Scholarship Council (CSC) scheme and the National Key Project of Fundamental Research and Development of China (No. 2011CB610306). The second author would like to acknowledge the financial support of the Royal Academy of Engineering.

References

[1] T. Igarashi, Characteristics of the flow around two circular cylinders arranged in tandem, *Bulletin of JSME* 24 (1981) 323–331.

[2] M.M. Zdravkovich, The effect of interference between circular cylinders in cross flow, *Journal of Fluids and Structures* 1 (1987) 239–261.

[3] M.M. Zdravkovich, *Flow around Circular Cylinders, vol. 1: Fundamentals*. Oxford University Press, Oxford, UK, 1997.

[4] M. Matsumoto, N. Shiraishi, H. Shirato, Aerodynamic instability of twin circular cylinders, *Journal of Wind Engineering and Industrial Aerodynamic* 33 (1990) 91-100.

[5] M.M. Zdravkovich, D.L. Pridden, Interference between two circular cylinders; Series of unexpected discontinuities, *Journal of Wind Engineering and Industrial Aerodynamic* 2 (1977) 255-270.

[6] N. Shiraishi, M. Matsumoto, H. Shirato, On aerodynamic instabilities of tandem structures, *Journal of Wind Engineering and Industrial Aerodynamic* 23 (1986) 437-447.

[7] M.M. Zdravkovich, Flow induced oscillations of two interfering circular cylinders, *Journal of Sound and Vibrations* 101 (1985) 511–521.

[8] J.C. Lin, Y. Yang, D. Rockwell, Flow past two cylinders in tandem: instantaneous and averaged flow structure, *Journal of Fluid and Structures* 16 (2002) 1059–1071.

[9] M.M. Zdravkovich, Review of flow interference between two circular cylinders in various arrangements, *Transactions of ASME Journal of Fluids Engineering* 99 (1977) 618–633.

[10] D. Sumner, Two circular cylinders in cross-flow: A review, *Journal of Fluids and Structures* 26 (2010) 849-899.

[11] L.N. Jenkins, M.R. Khorrami, M.M. Choudhari, C.B. McGinley, Characterization of unsteady flow structures around tandem cylinders for component interaction studies in airframe noise, *11th AIAA/CEAS Aeroacoustics Conference*, Monterey, AIAA Paper, 2005, pp. 2005-2812.

[12] L.N. Jenkins, D.H. Neuhart, C.B. McGinley, M.M. Choudhari, M.R. Khorrami, Measurements of unsteady wake interference between tandem cylinders, *36th AIAA Fluid Dynamics Conference and Exhibit*, San Francisco, AIAA Paper, 2006, pp. 2006-3202.

[13] F.V. Hutcheson, T.F. Brooks, Noise radiation from single and multiple rod configurations, *12th AIAA/CEAS Aeroacoustics Conference*, Cambridge, USA, AIAA Paper, 2006, pp. 2006-2629.

[14] D.P. Lockard, Summary of the Tandem cylinder solutions from the benchmark problems for airframe noise computations-I workshop, *49th AIAA Aerospace Sciences Meeting*, Orlando, Florida, AIAA Paper, 2011, pp. 2011-0353.

[15] M.R. Khorrami, M.M. Choudhari, D.P. Lockard, L.N. Jenkins, C.B. McGinley, Unsteady flowfield around tandem cylinder as prototype component interaction in airframe noise, *AIAA Journal* 45 (2007) 1930-1941.

[16] D.P. Lockard, M.R. Khorrami, M.M. Choudhari, F.V. Hutcheson, T.F. Brooks, Tandem cylinder noise predictions, *13th AIAA/CEAS Aeroacoustics Conference*, Italy, AIAA Paper, 2007, pp. 2007-3450.

[17] M.R. Khorrami, D.P. Lockard, M.M. Choudhari, L.N. Jenkins, D.H. Neuhart, C.B. McGinley, Simulation of bluff body flow interaction for noise source modeling, *36th AIAA Fluids Dynamics Conference and Exhibit*, San Francisco, AIAA paper, 2006, pp. 2006-3203.

[18] A. Uzun, M.Y. Hussaini, An application of delayed detached eddy simulation to tandem cylinder flow field prediction, *Computers & Fluids* 60 (2012) 71-85.

[19] G.A. Brès, D. Freed, M. Wessels, S. Noelting, F. Pérot, Flow and noise prediction for tandem cylinder aeracoustic benchmark, *Physics of Fluids* 24 (2012) 036101.

[20] H. Choi, W.P. Jeon, J. Kim, Control of flow over bluff body, *Annual Review of Fluid Mechanics* 40 (2008) 113-139.

[21] S.P. Yoo, D.Y. Lee, Time-delayed phase-control for suppression of the flow-induced noise from an open cavity, *Applied Acoustics* 69 (2008) 215-224.

[22] M. Gad-el-Hak, *Flow-control: Passive, Active, and Reactive Flow Management*, Cambridge University Press, Cambridge, UK, 2000.

[23] J.D. Revell, H.L. Kuntz, F.J. Balena, C. Horne, B.L. Storms, R.P. Dougherty, Trailing-edge flap noise reduction by porous acoustic treatment, *3rd AIAA/CEAS Aeroacoustics Conference*, AIAA Paper, 1997, pp. 1997-1646.

[24] M.R. Khorrami, M.M. Choudhari, Application of passive porous treatment to slat trailing edge noise, *NASA Report* TM-2003-212416.

[25] CH. Bruneau, I. Mortazavi, Passive control of the flow around a square cylinder using porous media, *International Journal for Numerical Methods in Fluids* 46 (2004) 415-433.

[26] CH. Bruneau, I. Mortazavi, Numerical modeling and passive flow control using porous media, *Computers & Fluids* 37 (2008) 488-498.

[27] D. Angland, X. Zhang, N. Molin, Measurements of Flow around a flap side edge with porous edge treatment, *AIAA Journal* 47 (2009) 1660-1671.

[28] T. Sueki, T. Takaishi, M. Ikeda, N. Arai, Application of porous material to reduce

aerodynamic sound from bluff bodies, *Fluid Dynamics Research* 42 (2010) 1-14.

[29] H.R. Liu, J.J. Wei, Z.G. Qu, Prediction of aerodynamic noise rduction by using open-cell metal foam, *Journal of Sound and Vibration*, 331(2012) 1483-1497.

[30] H. Naito, K. Fukagata, Numerical simulation of flow around a circular cylinder having porous surface, *Physics of Fluids* 24 (2012) 117102.

[31] Ansys Fluent 14.0 User's Manual, ANSYS Inc., Pennsylvania, USA, 2011.

[32] F.R. Menter, Improved two-equation k-ω turbulence models for aerodynamic flows, *NASA Report* TM 1992-103975.

[33] K. Vafai, Convective flow and heat transfer in variable-porosity media, *Journal of Fluid Mechanics* 147 (1984) 233-259.

[34] C.T. Hsu, P. Cheng, Thermal dispersion in a porous medium, *International Journal of Heat and Mass Transfer* 33 (1990) 1587-1597.

[35] B. Alazmi, K. Vafai, Analysis of variants within the porous media transport models, *Journal of Heat Transfer* 122 (2000) 303-326.

[36] S. Ergun, Fluid flow through packed columns, *Chemical Engineering Progress* 48 (1952) 89-94.

[37] S. Bhattacharyya, A.K. Singh, Reduction in drag and vortex shedding frequency through porous sheath around a circular cylinder, *International Journal for Numerical Methods in Fluids* 65 (2009) 683-698.

[38] Y. Bae, Y.J. Moon, Effect of passive porous surface on the trailing-edge Noise, *Physics of Fluids* 23 (2011) 126101.

[39] Y. Bae, Y.E. Jeong, Y.J. Moon, Computation of flow past a flat plate with porous trailing

edge using a penalization method, *Computers and Fluids* 66 (2012) 39-51.

[40] J.E. Ffowcs Williams, D.L. Hawkings, Sound generated by turbulence and surfaces in arbitrary motion, *Philosophical Transactions of the Royal Society* 264 (1969) 321–342.

[41] J.S. Cox, K.S. Brentner, C.L. Rumsey, Computation of vortex shedding and radiated sound for a circular cylinder: subcritical to transcritical Reynolds numbers, *Theoretical and Computational Fluid Dynamics* 12 (1998) 233–253.

[42] R.M. Orselli, J.R. Meneghini, F. Saltara, Twoandthree-dimensional simulation of sound generated by flow around a circular cylinder, *15th AIAA/CEAS Aeroacoustics Conference*, AIAA Paper 2009-3270.

[43] M. Zhao, L. Cheng, Finite element analysis of flow control using porous media, *Ocean Engineering* 37 (2010) 1357-1366.

[44] C.J. Doolan, Computational bluff body aerodynamic noise prediction using a statistical approach, *Applied Acoustic* 71 (2010) 1194-1203.

[45] N. Curle, The influence of solid boundaries upon aerodynamic sound, *Proceedings of the Royal Society of London, Series A, Mathematics and Physical Sciences* 231 (1955) 505-514.

Captions

Figure 1. Schematic of the tandem cylinders structure with porous covers in a uniform flow.

Figure 2. The C-type computational domain used for bare and porous-covered tandem cylinders.

Figure 3. The effect of thickness of the porous coating on the noise from tandem cylinders.

Figure 4. Comparison of noise spectra at Microphone B (9.11*D*, 32.49*D*) collected from various experimental and numerical investigations.

Figure 5. The effect of porosity of the coating on the noise from tandem cylinders.

Figure 6. Overall sound pressure level for tandem cylinder configuration with and without porous coating at three microphone positions: Microphone A at (-8.33D, 27815D), Microphone B at (9.11D, 32,49D) and Microphone C at (26.55D, 27.815D).

Figure 7. Time-averaged surface pressure coefficients on (a) upstream cylinder and (b) downstream cylinder.

Figure 8. RMS of surface pressure coefficients on (a) upstream cylinder and (b) downstream cylinder.

Figure 9. Time history of lift and drag coefficients on (a) upstream cylinder and (b) downstream cylinder.

Figure 10. Mean flow streamlines superimposed on total velocity magnitude normalized by U_∞ for (a) rigid case, (b) $h/R = 0.2,\ \phi = 0.95$, (c) $h/R = 0.3,\ \phi = 0.95$, (d) $h/R = 0.4,\ \phi = 0.95$.

Figure 11. Instantaneous spanwise vorticity magnitude, $|\omega_z| D/U_\infty$, for (a) rigid case, (b) $h/R = 0.2,\ \phi = 0.95$, (c) $h/R = 0.3,\ \phi = 0.95$, (d) $h/R = 0.4,\ \phi = 0.95$.

Figure 12. Mean turbulent kinetic energy normalized by U_∞^2 for (a) rigid case, (b) $h/R = 0.2,\ \phi = 0.95$, (c) $h/R = 0.3,\ \phi = 0.95$, (d) $h/R = 0.4,\ \phi = 0.95$.